Journal of Molecular Modeling (2023) 29:37
https://doi.org/10.1007/s00894-022-05438-8

ORIGINAL PAPER

Non-covalent interactions in the monohydrated complexes of 1,2,3,4–tetrahydroisoquinoline

Santu Das[1,2] · **Abhijit Chakraborty**[2]

Received: 11 November 2022 / Accepted: 23 December 2022 / Published online: 11 January 2023

Abstract

The eleven monohydrates of 1, 2, 3, 4-tetrahydroisoquinoline (THIQ) are analyzed through natural bond orbital (NBO) analysis and QTAIM methods employing M06-2X functional in DFT and MP2 methods. Here, the role of OH bonds as an acceptor and donor is critically analyzed. The role of lone pairs of O is critically monitored in two of the complexes, where N–H···O hydrogen bonds are present. The relative contributions of rehybridisation and hyperconjugation are compared in detail. Popelier criteria are satisfied in all the complexes barring a few exceptions involving weak hydrogen bonds. At the bond critical points (BCP), four monohydrates show higher values of electron density (ρ_C) and negative values of total electron energy density (H_C), while Laplacian ($\nabla^2\rho_C$) remains positive. These complexes satisfy the criteria of partial covalency. All these are O–H···N-type bonds. Remaining h-bonds are weaker in nature. These are also confirmed by the smaller values of ρ_C at the respective BCP. The variation of potential energy density (V_C) among the complexes seems to be the most important factor in determining the nature of non-covalent interactions.

Keywords Ab-initio calculations · 1,2,3,4 tetrahydroisoquinoline-water complex · Potential energy surface · Non-covalent interactions · NBO analysis · QTAIM

Introduction

Various kinds of non-covalent interactions play a major role in controlling a multitude of physical and chemical phenomena. The covalent interactions are conventionally represented by Lewis structures [1], which most of us experienced in our high school texts. Weaker non-covalent interactions on the other hand might arise from a variety of sources. Dispersion, dipole–dipole interactions, steric repulsions, and hydrogen bondings are a few of the prominent ones. The classic review by Kolman [2] discusses these parameters in great detail. Dispersive interactions play an important role from a wide range of microscopic to macroscopic phenomena. This weak attractive interaction is responsible for the "physiosorption" of gases in solids and is an important marker for characterizing bulk solids to nanomaterials [3]. This interaction is also responsible in explaining the adhesion of lizards on various surfaces [4] increasing its importance, although this is a weak interaction in nature. Dipole–dipole interactions are comparatively stronger than the dispersive ones, but among the non-covalent interactions, hydrogen bonding had stolen the limelight for the last few decades. Its variety and the range of applications from the microscopic world [5] to the extreme environments in interstellar media [6] continue to fascinate scientists and people in general.

On the per-atom basis, hydrogen bonding is the strongest among all the non-covalent interactions. The structure of proteins [7] and DNA [8] can only be explained by this non-covalent interaction. The hydrogen bonding is defined as X–H···Y, where the hydrogen atom (H) is placed in between the two electronegative atoms (X and Y). Y atom should have one or multiple lone pairs or appropriate electron distribution to form the H···Y bond. This bonding involves the physical transfer of electronic charge from the lone pair of Y atom (Lewis base) to the σ^* orbital of the X–H bond (Lewis acid) changing the atomic characteristics of the individual atoms on the formation of the bond. One may also view this as a transfer of a proton from a hydrogen bond donor (X) to the acceptor (Y) site. Since the bonding characteristics of the H atom are

✉ Abhijit Chakraborty
achakraborty.buphys@gmail.com;
achakraborty@phys.buruniv.ac.in

[1] Department of Physics, Government General Degree College, Hooghly, Singur 712409, India

[2] Department of Physics, The University of Burdwan, Golapbag Campus, Burdwan 713104, West Bengal, India

different with these two atoms X and Y, even if X and Y are identical, we will observe some interesting phenomenon. The problem of understanding the non-covalent interactions becomes complicated if there are multiple sites of hydrogen bonding, mainly with the variation of Y. The strength of hydrogen bonding can vary over a large range with the variation of atomic properties of X and Y and also the neighborhoods of them. Numerous reviews [9–14] dealing with and comparing the strength of this h-bonding are available. The strength is also connected with the directionality of this bond mainly defined by the angle ∠XHY. The more linearity in orientation favors the strongest bonds. The covalency of the strongest of the hydrogen bonds arouses a lot of interest [9].

The nature of hydrogen bonds (HB) can be explored from various perspectives. Mere comparison of binding energies might not be the best idea to get hold of the problem. Natural bond orbital (NBO) analysis [15] deals with the wavefunctions of the optimized structures having HBs. It pictorially shows the different molecular orbitals involved in the intramolecular or intermolecular hydrogen bonding. This is mainly done in following $n_Y \rightarrow \sigma_{XH^*}$ orbital overlap energy. The beauty of this analysis is one can follow all the bonds of the participating molecules individually to understand how this bonding affects even those regions of a molecule which are not directly involved in this non-covalent interaction. One can also follow the characteristics of the atoms taking part in this bonding in an elegant way. This paved the way for a facile observation of charge transfer and the formation and breaking of hydrogen bonds. This analysis also gives us the changes occurring in the hybridization characteristics in the hydrogen bond donor during the whole process. A number of problems were successfully solved by this analysis [16–18].

Quantum Theory of Atoms in Molecules [QTAIM] [9, 18–21] is another approach which provides us with geometrical, topological, and energetic characteristics of various kinds of hydrogen bonds [22, 23]. According to this theory [18, 19], nuclei are considered as attractors defined as the gradient vector field of charge distributions. These are denoted as $(3,-3)$ critical points having maxima of charge density. An atom is looked upon as a union of an attractor (nucleus) and its associated basin (electron density distribution). Here, the electron density (ρ) is plotted in the region occupied by the atoms in the molecules; consequently one can visualize the bond path connecting the atoms. At the bond critical point (BCP) Hessian matrix of the charge density has two negative and one positive eigenvalues. These are denoted as $(3,-1)$. At these points, ∇ρ vanishes. The respective value of ρ at these points is termed ρ_C. Similarly, for a ring, we get ring critical points (RCP) denoted as $(3,+1)$. The nature of the bonds is characterized by the values of ρ and its second derivative or Laplacian ($\nabla^2\rho$). The corresponding eigenvalues of the Hessian matrix and the sign of Laplacian indicate the nature of the non-covalent interactions [9]. For non-covalent interactions between two atoms, if the electron density reduces in the interatomic region, Laplacian will be positive which indicates dipole–dipole, van der Waals, and conventional hydrogen bonds in general. But, if Laplacian becomes negative, it hints at an accumulation of charges and consequent electron density in that region. It implies sharing of electron charges and points to a covalent nature of the corresponding non-covalent interaction [9]. It needs to be mentioned that the characteristics of energy at the BCP are connected with the Laplacian through the following relations:

$$\frac{1}{4}\nabla^2\rho_C = 2G_C + V_C$$

$$H_C = G_C + V_C$$

where H_C, G_C, and V_C are the total electron energy density, the kinetic electron energy density, and the potential electron energy density, respectively. Here, G_C is always positive and V_C is negative, making the sign and value of H_C as an indicator of the nature of bonding. Strong hydrogen bonds are characterized by positive values of $\nabla^2\rho_C$ and negative values of H_C. When both of them appear with positive values then it is a moderate to weak h-bonding [9]. On the other hand, extreme negative values of both $\nabla^2\rho_C$ and H_C indicate very strong hydrogen bonding. This can also be looked at as h-bonding with covalent characteristics [9]. According to the AIM approach, the topological criteria for the existence of hydrogen bonding were put forward by Popelier [24]. These criteria include (i) the correct topological pattern for bond path and BCP, (ii) a relatively high value (0.002–0.034 a.u.) of $\rho_{H\cdots Y}$ (at the H atom of the H···Y hydrogen bond) at the BCP, (iii) $\nabla^2\rho_{H\cdots Y}$ should be within the range 0.024–0.139 a.u. at BCP, (iv) the formation of hydrogen bonding will be revealed by the mutual penetration of H atom and acceptor atoms, (v) evidence of loss of charge on H atom on hydrogen bond formation, (vi) destabilization in the energy of H atom on bonding, (vii) decrease in dipolar polarization of H atom on the formation of cluster, and (viii) decrease in the volume of hydrogen atom due to intermolecular interaction.

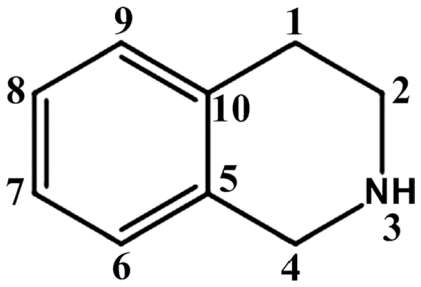

THIQ

In this paper, we will find out the non-covalent intermolecular interactions present in the monohydrated complexes of 1, 2, 3, 4-tetrahydroisoquinoline (THIQ). TA, TE, and BA are the conformers of bare THIQ molecule [25], where T stands for "twisted" and B for "bent" conformations of the saturated ring. "Axial" and "Equatorial" orientations of the NH bonds in the above conformations are indicated by A and E, respectively. Recently, we explored the different conformations of the THIQ:(H_2O) [26] and THIQ: (NH_3) [27] complexes in S_0. We also succeeded in reassigning the IR-UV and UV-UV double resonance spectra [28] of the monohydrated complex [25]. Bare THIQ poses different conformations in S_0. TA and TE are the two close-lying structures [25, 29] in S_0. There is some ambiguity [25] in the determination of the global minimum in S_0. But, when conformer selective water complexes were studied [28], it is unambiguously observed and corroborated experimentally that the monohydrates with the twisted equatorial (TE) configuration of THIQ are the global minimum. The other close-lying monohydrated complex with the twisted axial (TA) conformer lies about 200 cm^{-1} higher than the corresponding complex in the TE form. In the former, both the OH bonds of water participate in the h-bonding as O–H···N and O–H···π type,while in the latter O–H···N type is only present. Although the H bond length is not shorter in the TE form, the overall contribution from the two HBs energetically separates the conformer selective water complexes and $(THIQ)_{TA}$: (H_2O) becomes the global minimum in the potential energy surface (PES) [26] of the cluster study. Apart from TE and TA forms, the bare THIQ [25] also shows a bent conformation of the saturated ring in the axial configuration of the N atom, termed as bent axial (BA) form. This is located about 700 cm^{-1} higher in energy. The other bent form bent equatorial (BE) is interestingly a transition state (TS) in the bare molecule [25]. In monohydrates of THIQ, the BE conformer forms the complex with the largest binding energy [26], even larger than the TE and TA forms. This raises a lot of questions and we feel it necessary to distinguish the nature of hydrogen bonding on the basis of QTAIM theory to enquire about the possibility of covalency [9] in any of the conformer selective monohydrates of THIQ. We also observed that the behavior of the two OH bonds in the complexes was different. Out of the two OH bonds of water, the one not participating in the H bonding behaves quite differently from the participating one in the TE conformer of THIQ. As, we focused mainly on the identification of different conformers and reassigning the vibrational spectrum in our earlier work, here we will try to explore these monohydrated complexes in greater detail.

The questions this paper will try to address are:

1. Is there any of the monohydrates of THIQ that show covalency character as classified by QTAIM computations and aptly described by Grabowski et al. [22]?
2. Do all the monohydrates follow the criteria proposed by Popelier [24]?
3. In our earlier article [26] we observed a difference in the behavior of two OH bonds of water on hydrogen bonding. Will the behavior of free (not participating in hydrogen bonding) OH bonds remains identical irrespective of the behavior of the O atom as an acceptor or donor of H bonds?
4. Does the hydrogen bonding behavior change identically as that observed [26] in TA and TE forms of THIQ when the role of donor and acceptors are interchanged?
5. How far can we distinguish different kinds of hydrogen bonding interactions on the basis of different properties at BCP?

Computational methods

We will use both Density Functional theory (DFT) [30] as well as 2nd order Moller–Plesset perturbation theory, MP2 [31] methods. Within the DFT framework, M06-2X functional [32] will be utilized here for describing these non-covalent interactions. The suitability of this functional over other functionals in these types of cases was well documented and also observed in our earlier works [26]. The basis set 6-311G + + (2d, 3p) [33] is used in both these methods. All the different structures of these complexes are computed in Gaussian 09 [34] suits of the program. The wavefunctions of different optimized complexes were used in natural bond orbital (NBO) analyses. This is achieved through NBO 3.1 associated with Gaussian09. AIM analysis has been done with the help of Multiwfn [35].

Results and discussions

In our previous work, [26] we observed 11 distinct monohydrated complexes of THIQ. There are multiple centers of h-bondings in THIQ. We had classified [26] these different HBs according to the primary HB centers. There are three different types of HBs where the primary HB centers are—(a) O–H···N, (b) N–H···O, and (c) O–H···π. Apart from these primary centers, we observed secondary HBs in some of the complexes. The nomenclature of the different complexes will remain identical as earlier [26]. Respective monohydrates for TE conformation of THIQ were coined as TEW1a, TEW1b, TEW1c, and respectively so for TA, BA, and BE conformers of bare THIQ.

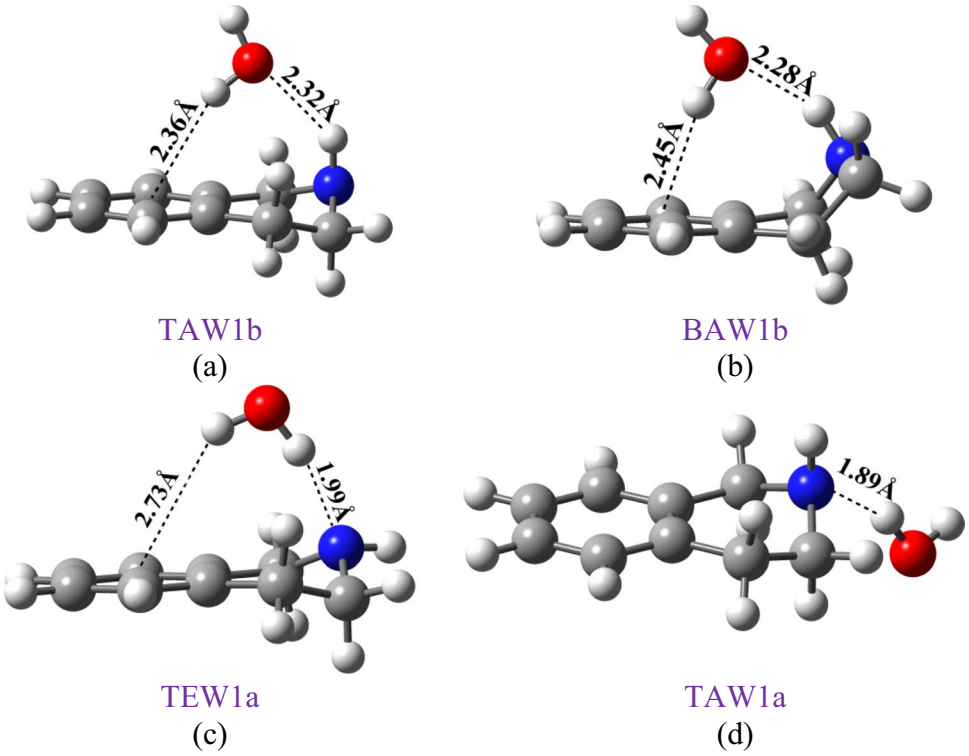

Fig. 1 The important complexes of THIQ: H_2O **a** TAW1b, **b** BAW1b, **c** TEW1a, and **d** TAW1a. Computations are performed at M06-2X/aug-cc-pVDZ level of theory

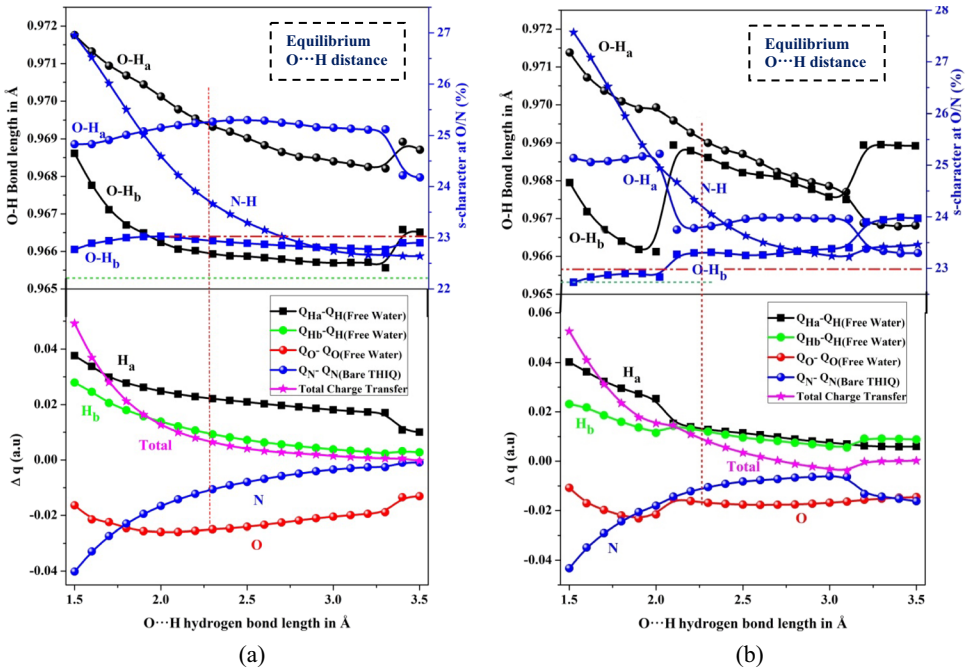

Fig. 2 Correlations of charge transfer, change in O–H bond length, and the change of s-character (%) of O–H bond at O due to $n_O/\pi_{C\text{-}C} \rightarrow \sigma^*_{(O\text{–}H)}$ interactions with O···H-N H-bond length of two complexes **a** TAW1b and **b** BAW1b. The vertical line indicates the H-bond length at the equilibrium geometry and horizontal lines indicate % of s-character and O–H bond length of bare H_2O. Computations are performed with M06-2X/aug-cc-pVDZ level

NBO analysis

The different intra- and intermolecular interactions within a pair of covalent bonds (A-H···X-B) related through hydrogen bonding were conveniently probed by NBO analysis [18]. Here the X usually has one or multiple lone pairs. This is an important analytical tool for understanding non-covalent interactions. This analysis assesses the relative contribution of two different factors involved in hydrogen bonding–- (i) hyperconjugation following the electronic charge transfer (Q_{CT}) from the filled lone pair orbitals (n_X) in X to the empty anti-bonding orbital (σ_{AH}^*) of the HB donor (A-H)

Table 1 Comparison of the change of NBO charges (a.u), bond lengths (Å), and angle (degree) of involved atoms due to the formation of H-bond from its bare molecules for all the monohydrates of THIQ. Computations are performed at M06-2X/aug-cc-pVDZ level of theory

Complexes	Change of O-H_a	Change of O-H_b	Change of charge at H_a	Change of charge at H_b	Change of charge at O	Change of H_a-O-H_b angle
TEW1a	0.01229	0.00102	0.01600	−0.00432	−0.03539	−0.785
TAW1a	0.01606	−0.00167	0.02278	−0.00307	−0.04946	1.186
BAW1a	0.01671	−0.00167	0.02401	−0.00285	−0.05066	1.183
BAW1a*	0.01665	−0.00169	0.02466	−0.00033	−0.05104	1.363
BEW1a	0.01360	0.00097	0.01792	−0.00513	−0.03767	−0.722
TEW1b	0.00082	0.00042	0.01023	0.00878	−0.01228	0.469
TAW1b	0.00400	0.00035	0.01574	0.01040	−0.02079	0.653
BAW1b	0.00437	0.00021	0.01546	0.00966	−0.01943	0.519
TEW1c	0.00256	0.00134	0.00322	0.00123	−0.00464	−2.136
TAW1c	0.00301	0.00070	0.00427	0.00220	−0.00596	−1.790
BAW1c	0.00217	0.00154	0.00285	0.00192	−0.00439	−2.054

and (ii) rehybridization depicting the change in hybridization characteristics in the donor. In our previous publication on this complex [26], we analyzed the NBOs in the two lowest energy complexes, TEW1a and TAW1a only. It is to be noted that both the studied complexes are of "a" type, where O–H···N is the primary HB. Hyperconjugation was the predominant mechanism. The behavior of individual OH bonds of water was thoroughly probed. If any of the two OH bonds of water remains "free" (non-participation in h-bonding), it behaved differently from the other one. The former OH bond was found to shorten on HB. It was observed only in the TAW1a complex. We also looked at bond-specific non-covalent interactions in those complexes. We observed that energy associated with NBO (E_{NBO}) accounts for this quite well.

Apart from the above-mentioned two complexes, we found that TAW1b, TAW1c, TEW1b, BAW1a, and BAW1b complexes have at least one "free" OH bond in water. We will study these in greater detail and try to verify and conclude on the behavior of "free" OH bonds in the monohydrates of THIQ. The bonded H atom in water is termed H_a and the "free" one H_b. Some common features observed earlier in TAW1a and TEW1a complexes were —(i) The O-H_b bond length (BL) decreases when H_b is free, (ii) the O-H_a BL increases in all cases including the case when H_b is not "free", and (iii) charges on H_a (when free) increases and H_b decreases on complexation. The changes were more pronounced in TAW1a than TEW1a, (iv) Charge on O atom decreases and the change was more in TAW1a. In both these complexes, the OH bonds behave as HB donor while N lone pair as acceptor. But within the above-mentioned complexes, TAW1b, BAW1b, and TEW1b complexes show N–H···O type h-bond signifying the reversal of the role of N and O atoms in this HB. Then, NH bond will behave as a donor and lone pair of O atom as HB acceptor. The C-H···O bonds are weakest among all the h-bonds here and we left out those complexes where they appear as a primary or secondary HBs. Since BAW1a and BAW1a* bear the same signature of H bonding as TAW1a, we will leave them out of this discussion here. Similarly, TEW1a has its identical counterparts as BEW1a, TEW1c, and BAW1c and we will not explore the behavior of OH bonds in these complexes. Considering all these aspects we will thoroughly investigate the HBs in TAW1b and BAW1b only shown in Fig. 1 computed at M06-2X/aug-cc-pVDZ level. Corresponding results with M06-2X/6–311 + + G (2d, 3p) level and respective coordinates are given in figures. F1 and F2 respectively in the supplementary file. Consistency in the results is noteworthy.

In both cases, the primary HB is N–H···O type [26] as clearly evident from the values of equilibrium H-bond lengths. In both TAW1b and BAW1b, there is an additional O–H···π bond. We follow both the O–H bonds in these two complexes as we vary the N–H···O bond lengths. The H···O hydrogen bond lengths are varied from a value smaller than the equilibrium bond lengths and extended up to the point where H-bond disappears. We also closely watch the lone pairs on the O atom, whether they are forming any new H bonds or not. The change in the s-character of the O atom on h-bonding is also calculated to ascertain which interaction among rehybridization and hyperconjugation dominates here. These plots are shown in Fig. 2.

Figure 2 shows the variation of O···H-N hydrogen bond lengths in TAW1b and BAW1b complexes over a range of 1.50 Å to 3.50 Å. The corresponding equilibrium bond lengths are around 2.30 Å. Due to hyperconjugative interaction electronic charge is transferred to the N–H bond from O. On the other hand, weak O–H···π bond signifies a transfer of charge from π electrons to an O–H bond. So, some competitive processes are going on here as we change the O···H-N bond lengths. In TAW1a and TEW1a, NH bonds do not form

any h-bonds with lone pairs of O atom. So, charge transfer from O was not feasible [26].

For TAW1b (Fig. 1a), as the N–H···O bond length is increased the charge transfer to the N–H bond also decreases, consequently, the charge on O decreases and charge on N increases from the equilibrium value. Interestingly with this increase in this BL, O-H_a···π bond length decreases and charge is transferred to O-H_a bond. So, after the initial decrease charge on the O atom increases.

Change of charges (ΔQ) at H_a and H_b is decreasing continuously with the increase of N–H···O length, but the rate of change is different. Sudden change of charge at H_a and O is observed close to 3.40 Å. This is due to the development of a weak C2-H···O bond with the increase of H···O BL. This effect is prominently observed in O-H_a bonds signifying the difference in H_a and H_b atoms. Consequently, hybridization character changes. The change in % of the s-character at O and its charge changes consistently. In case of the N–H bond, the s-character at N continuously decreases which is natural as the h-bond length increases. The % of the s-character at the electronegative atom involving HB should decrease according to Bent's rule [36].

In BAW1b (Fig. 1b), similar phenomena are observed apart from some sudden change. With the increase in N–H···O bond lengths, water shifts more towards the pi-electron cloud, and the C2-H···O bond is formed much more easily than in TAW1b. O-H_b increases more than O-H_a when N–H···O is about 2.10 Å as it comes closer to π-electrons cloud and the orientation of H_2O changes. As N–H···O is shifted to a BL around 3.20 Å, H_2O is shifted towards C2-H and C2-H···O HB is formed. Interestingly, as the shifts progress the O-H_a shifts to the side of the benzene ring, and O-H_b···π become more prominent than O-H_a···π which was more in earlier case. All these things are clearly and consistently indicated by the change of charge, O–H lengths, and % of s-character.

In "a" type complexes (e.g., TAW1a and TEW1a), OH bonds acted [26] as HB donors, while in "b" type one like TAW1b and BAW1b these bonds act both as a donor and acceptor. The relative strength of HBs changes with the type of complex formed. With the increase in N–H···O BLs the O-H_b bonds showed an increase in the "a" types [26], while this is not observed here. The involvement of that bond at higher N–H···O BLs might also be a reason to be probed later. The different kind of trend is also observed for "a" and "b" types of complexes in the changes in charges (ΔQ) over H_a and H_b atoms. ΔQ and change in % s-character at O atom in "a" type complexes were discussed [26] in detail and it was concluded that hyperconjugation predominates rehybridisation. Here, in these "b" type complexes ΔQ over both the H atoms decrease with the increase in N–H···O BLs, but as O–H bond length decreases % of s-character at

Table 2 The NBOs which are involved in hydrogen bonding interactions in all monohydrates of THIQ and their E_{NBO} (kcal/mol), s-character, and bond polarization (%) associated with O atom and corresponding values of bare H_2O molecule and total charge transfer (a.u). Analysis has been performed at M06-2X/aug-cc-pVDZ level

Complexes/monomer	Interacting orbitals	E_{NBO}	% of s-character at O/N	Bond polarization	Q_{CT}
TEW1a	$n_N \rightarrow \sigma^*_{(O\text{-}Ha)}$	10.27	27.92	76.33	−0.0237
	$\pi_{(C5\text{-}C10)} \rightarrow \sigma^*_{(O\text{-}Hb)}$	0.34	22.79	74.07	
TAW1a	$n_N \rightarrow \sigma^*_{(O\text{-}Ha)}$	13.60	28.59	76.83	−0.0259
H_2O*			23.57	74.31	
BAW1a	$n_N \rightarrow \sigma^*_{(O\text{-}Ha)}$	14.25	28.66	76.88	−0.0295
BAW1a*	$n_N \rightarrow \sigma^*_{(O\text{-}Ha)}$	13.76	28.60	76.86	−0.0267
BEW1a	$n_N \rightarrow \sigma^*_{(O\text{-}Ha)}$	11.88	28.01	76.41	−0.0249
	$\pi_{(C9\text{-}C10)} \rightarrow \sigma^*_{(O\text{-}Hb)}$	0.33	22.22	74.05	
TEW1b	$n_O \rightarrow \sigma^*_{(N\text{–}H)}$	2.56	22.82(N)	70.99	0.0067
	$n_O \rightarrow \sigma^*_{(C\text{-}H)}$	0.01			
TAW1b	$n_O \rightarrow \sigma^*_{(N\text{–}H)}$	3.31	22.93(N)	70.67	0.0054
	$\pi_{(C5\text{-}C10)} \rightarrow \sigma^*_{(O\text{-}Ha)}$	1.60	25.45	75.25	
BAW1b	$n_O \rightarrow \sigma^*_{(N\text{–}H)}$	3.01	23.32(N)	70.91	0.0057
	$\pi_{(C5\text{-}C6)} \rightarrow \sigma^*_{(O\text{-}Hb)}$	1.09	25.51	75.23	
TEW1c	$\pi_{(C6\text{-}C7)} \rightarrow \sigma^*_{(O\text{-}Hb)}$	0.72	24.01	74.54	0.0005
	$\pi_{(C8\text{-}C9)} \rightarrow \sigma^*_{(O\text{-}Hb)}$	0.35	23.40	74.37	
TAW1c	$\pi_{(C5\text{-}C10)} \rightarrow \sigma^*_{(O\text{-}Hb)}$	0.74	24.46	74.66	-0.0002
	$n_O \rightarrow \sigma^*_{(C\text{-}H)}$	0.23			
BAW1c	$\pi_{(C5\text{-}C6)} \rightarrow \sigma^*_{(O\text{-}Hb)}$	0.66	23.80	74.49	0.0004
	$\pi_{(C9\text{-}C10)} \rightarrow \sigma^*_{(O\text{-}Hb)}$	0.68	23.60	74.42	
TE #			21.92(N)	69.68	
TA#			21.80(N)	69.28	
BA#			21.95(N)	69.44	

*Bare H_2O molecule. The first two rows are reproduced from Ref[26]

#Comformers of Bare THIQ

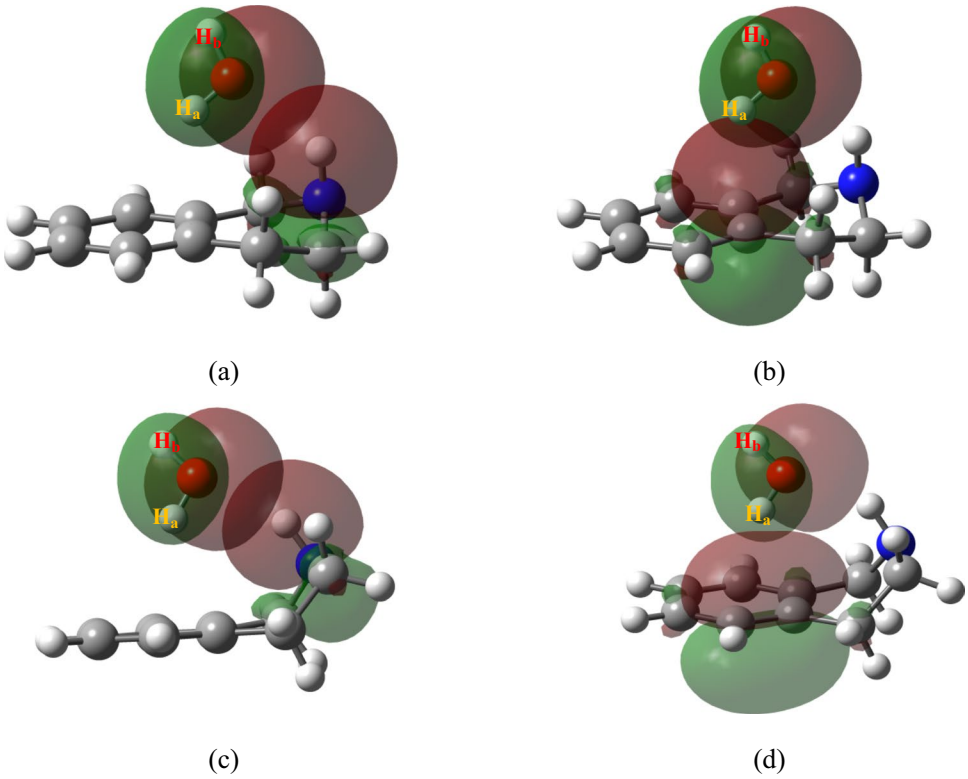

Fig. 3 Natural bond orbitals displaying the overlap between donor and acceptor orbitals of TAW1b complex for **a** N–H···O and **b** O–H···π hydrogen bonding interactions. Corresponding orbitals for the BAW1b complex are in **c** N–H···O and **d** O–H···π. Analysis has been performed with M06-2X/6–311 + + G (2d, 3p) level for an isovalue of 0.02

O increases. At 2.10 Å in BAW1b complex, there is a change in orientation of water molecules, which is displayed as a sudden change in all the quantities in this complex. These indicate that rehybridisation predominates hyperconjugation in these complexes.

Table 1 lists the change in O-H_a and O-H_b bond lengths of water for all the monohydrates of THIQ computed at M06-2X/aug-cc-pVDZ level. The corresponding computations with M06-2X/6–311 G + + (2d, 3p) are in Table T1 in the supplementary file. The results are quite consistent. These tables also contain changes on NBO charges and the H_a-O-H_b angles. Changes are measured with respect to the values in bare water molecule. The O-H_b bond lengths always decreased for all "a" type complexes when O-H_b was free and O-H_a forming strong O–H···N HB [26]. The H_a-O-H_b angles increase for all "a" and "b" types of complexes other than two complexes [TEW1a and BEW1a] where a π-bond is associated with O–H···N h-bond. These changes in O-H_b BLs and H_a-O-H_b angles in these complexes are quite different from other complexes. These changes are also reflected in the atomic properties of involved individual atoms.

In these monohydrates of THIQ, we have lone pairs of N/O atoms as well as π electron clouds of the unsaturated rings interacting with various anti-bonding orbitals of the O–H/N–H/C-H bonds. The interaction energy is measured through E_{NBO}. It is calculated as a second-order perturbation energy [18]. If we consider the lone pairs from the N atom and the anti-bonding orbital (σ^*) of the OH bond, then it can be expressed as.

$$E_{NBO}(n_N \rightarrow \sigma^*_{OH}) = -q\frac{\langle \psi_n | F | \psi_{\sigma^*} \rangle}{\epsilon_{\sigma^*_{OH}} - \epsilon_{n_N}}$$

where q is the donor orbital occupancy and generally considered to be close to two, F is the Fock operator and $\epsilon_{\sigma^*_{OH}}$ andϵ_{n_N} are the energy eigenstates corresponding to the molecular orbitals ψ_n of nitrogen atom and $\psi_{\sigma^*_{OH}}$, respectively. This expression is suitably applied for other combinations of lone pairs and anti-bonding orbitals, respectively. Complexes having multiple HBs will have multiple contributions. Table 2 lists the computed values of E_{NBO} for all the complexes detailing each individual contributions. This table also includes bond polarization, the amount of charge transfer, and values of the s-character of O atoms. According to this table, the s-character of the O atom increases in the respective complexes. Similarly, the s-character of the N atom increases in the respective complexes, where N–H···O h-bonds are involved, which validates Bent's rule [36]. Table T2 in the supplementary file computes these parameters with 6–311 + + G (2d, 3p) basis. Results remained consistent as earlier.

If E_{NBO} of these complexes is compared with binding energies (BE) [26], a discernible pattern is noticed. The maximum in both BE and E_{NBO} appeared for "a" type of complexes. But, among the complexes within this category, the ones connected with the equatorial conformation of THIQ have the highest value in BE which might be arising

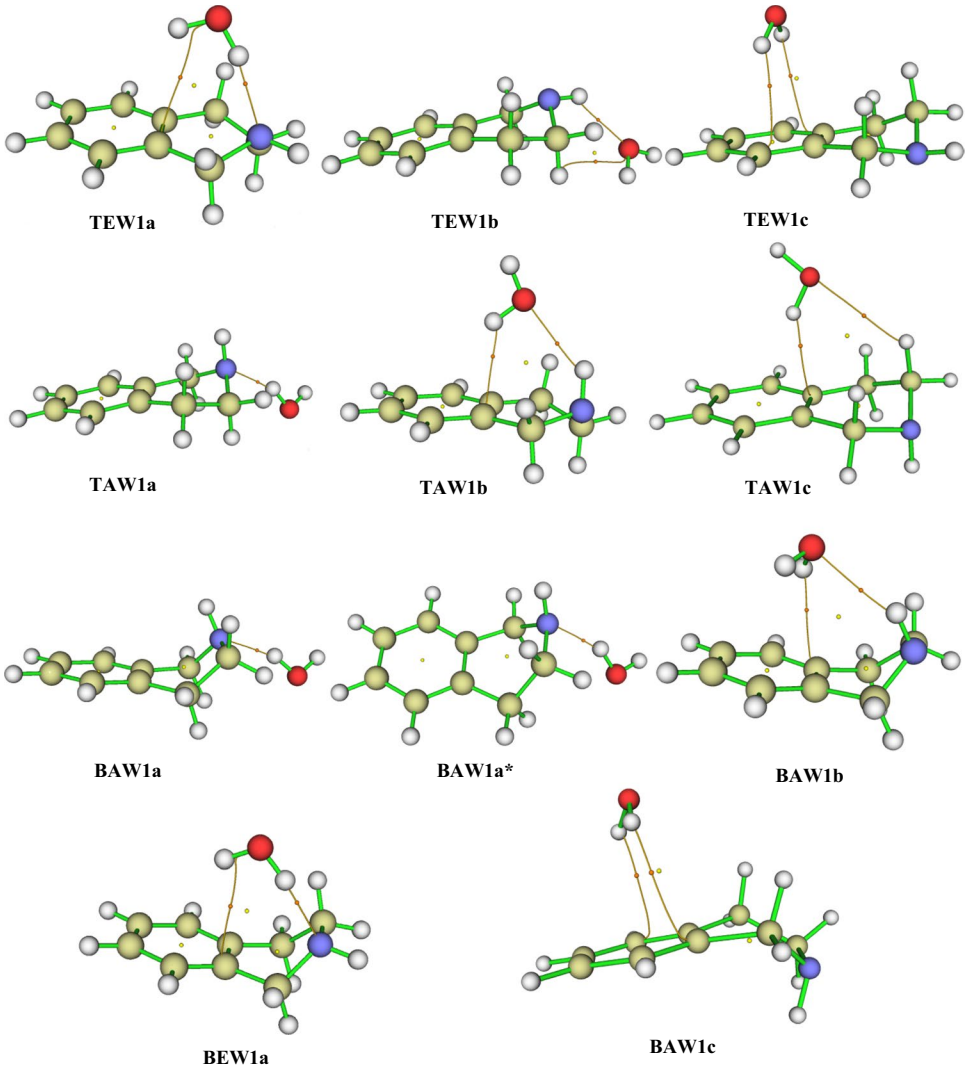

Fig. 4 Molecular topography analysis of THIQ: H_2O complexes as obtained from theoretical electron density. Bond critical point and ring critical point are denoted by orange dots and yellow dots, respectively

from the multiple HBs associated with these kinds of structures. On the contrary, the axial conformations of bare molecule possess the highest values of E_{NBO}. This might be due to the shorter HB lengths in these complexes producing largest amount of charge transfer.

The plots of the involved atomic orbitals in these two complexes are shown in Fig. 3. The participating atomic orbitals in TAW1b cluster are shown in Figs. 3a and b. The overlap is more pronounced in O···H HBs shown in Fig. 3a. While a close look at the weak HB involving π electron clouds of unsaturated ring displays the involvement of only C5 and C10 in TAW1b and C9 and C10 in BAW1b. Charge on both carbon atoms is found to decrease and the respective C–C BLs increase, as it is observed in O–H bonds in the acceptor site for both complexes. The change of charges and bond lengths are provided in Table T3 in the supplementary material. The H-bond distances for this category will henceforth be measured from the midpoint of that specific C–C bond of the ring. The respective plots in BAW1b complex are shown in Fig. 3c and d, where the O atom simultaneously acts as a donor as well as an acceptor.

AIM results

This approach is successfully applied in numerous problems [9, 19–21, 37] to recognize the topological features of hydrogen bonding. In our earlier work [26] we had identified the presence of single and multiple h-bonds in TAW1a and TEW1a, respectively. Apart from computational works, the IR-UV double resonance experiments [28] also amply show a shift in NH stretching modes in these two complexes. The analysis of the shifts [26] clearly indicated the presence of additional hydrogen bonding in TEW1a cluster, which was later confirmed as O–H···π type. With this nice corroboration of our computational works, we are now in a position to apply these works for the entire set of monohydrates. Earlier, we had listed all the hydrogen bonds in all the complexes

Table 3 N–H covalent and H···N non-covalent bond lengths (both are in Å) and their different topological parameters, Electron density (ρ_C) at BCP, its Laplacian $(\nabla^2\rho_C)$, kinetic electron energy density (G_C), potential electron energy density (V_C), and total electron energy density (H_C) (all are in a.u) for all THIQ: H_2O complexes calculated at M06-2X/6–311 + + G(2d,3p) level

Complexes	Involved atoms	N–H(H···N)	ρ_c	$\nabla^2\rho_c$	G_C	V_C	H_C
TEW1a	N–H	1.0107	0.3505	− 1.6447	0.0666	− 0.5443	− 0.4777
	O–H···N	1.9963	0.0272	0.0816	0.0198	− 0.0193	0.0006
TAW1a	N–H	1.0137	0.3476	− 1.5990	0.0671	− 0.5339	− 0.4668
	O–H···N	1.8960	0.0334	0.0938	0.0251	− 0.0267	− 0.0016
BAW1a	N–H	1.0113	0.3512	− 1.6443	0.0671	− 0.5453	− 0.4782
	O–H···N	1.8827	0.0344	0.0948	0.0258	− 0.0279	− 0.0021
BAW1a*	N–H	1.0091	0.3524	− 1.66	0.0677	− 0.5504	− 0.4827
	O–H···N	1.8942	0.0334	0.0966	0.0256	− 0.0271	− 0.0015
BEW1a	N–H	1.0091	0.3515	− 1.6563	0.0649	− 0.5491	− 0.4816
	O–H···N	1.9590	0.0293	0.0867	0.0217	− 0.0218	− 0.0001
TEW1b	N–H	1.0113	0.3511	− 1.7000	0.0645	− 0.5540	− 0.4895
	N–H···O	2.2757	0.0130	0.0486	0.0105	− 0.0089	0.0016
TAW1b	N–H	1.0145	0.3475	− 1.6510	0.0649	− 0.5426	− 0.4777
	N–H···O	2.3383	0.0116	0.0407	0.0089	− 0.0077	0.0012
BAW1b	N–H	1.0130	0.3502	− 1.6841	0.0650	− 0.5512	− 0.4861
	N–H···O	2.4467	0.0119	0.0381	0.0085	− 0.0074	0.0011
TEW1c	N–H	1.0103	0.3506	− 1.6324	0.0678	− 0.5436	− 0.4760
TAW1c	N–H	1.0129	0.3476	− 1.5856	0.0685	− 0.5334	− 0.4649
BAW1c	N–H	1.0112	0.3509	− 1.6288	0.0684	− 0.5441	− 0.4756

just from the optimized geometries of the quantum chemical computations. We were confident about the moderate to strong h-bonds, but not so for the weak ones and particularly those bonding with the π electron clouds of the unsaturated ring of THIQ. So, it becomes necessary to extend our work for all the complexes of THIQ to explore the quantitative nature of all the hydrogen bonds. In this respect, the AIM method comes handy and expects to ascertain our earlier observations.

The topography of all the complexes is shown in Fig. 4. The existence of multiple HBs is distinguished by the presence of multiple BCPs and their respective associated parameters. In these cases, all the bond critical points (3, − 1) and ring critical points (3, + 1) are easily identifiable. The O–H···π interactions are also identified in the respective complexes. The presence and location of BCPs indicate the nature of this kind of intermolecular interactions as hydrogen bonding. The values of electron density(ρ_C), its Laplacian$(\nabla^2\rho_C)$, total electron energy density (H_C), kinetic electron energy density (G_C), and potential electron energy density (V_C) are shown in Table 3 for the H···N pair of interatomic atoms for all the complexes. This include (i) NH covalent bonds for N–H···O hydrogen bridges involving lone pair of O atom in the hydrogen bonding and (ii) O–H···N in hydrogen-bonded systems involving nitrogen lone pair. Table 4 includes the corresponding values involving O···H pairs of atoms. In the case of covalent NH bonds, shorter bond lengths in the range of 1.0091–1.0145 Å, a high value of electron density at BCP along with negative values of Laplacian are noted. In all the N–H and O–H bonds both H_C and $\nabla^2\rho_C$ is negative, satisfying the ideas put forward earlier. On the other hand, in all the hydrogen bonds $\nabla^2\rho_C$ although remains positive, we find a difference in the nature of H_C. Apart from the TEW1a cluster, in all other O–H···N hydrogen bonds, H_C remains negative, indicating strong hydrogen bonding. But H_C remains negative for all O–H···N hydrogen bonds in MP2 computation. H-bonds remain weak in all O–H···π bonds, confirmed by the positive nature of H_C. One can also guess about the strength through the respective values of ρ_C. Although TEW1a is one of the most stable monohydrates, its strength is enhanced through the presence of an additional O–H···π bond. Another interesting complex is BEW1a. Although BE is a transition state in bare THIQ, this complex has one of the largest binding energy among all the monohydrates, making it somewhat special [26]. In this case, O–H···N h-bond length is slightly smaller than TEW1a, which makes H_C negative through the increase of ρ_C. The variation of $\nabla^2\rho_C$ and H_C with ρ_C is shown in Fig. 5. Strong and weak h-bonds are clearly separated out in this plot. At a value of $\rho_C = 0.0285$ we can observe a change over from weak to strong h-bonding with the transformation of the sign of H_C. Considering primary bond lengths only, ρ_C is linearly proportional to bond lengths. This can also be inferred from Figure F3 in the supplementary file. Here, we can assume that strong non-covalent interactions are expected to appear for hydrogen bond lengths approximately shorter than 1.96 Å. Lower than this value of BL as well as the corresponding value of ρ_C, H_C becomes negative,

Table 4 O–H covalent and H···O non-covalent bond lengths (both are in Å) and their different topological parameters, Electron density (ρ_C) at BCP, its Laplacian $(\nabla^2\rho_C)$, kinetic electron energy density (G_C), potential electron energy density (V_C), and total electron energy density (H_C) (all are in a.u) for all THIQ: H_2O complexes calculated at M06-2X/6–311 + + G(2d,3p) level

Complexes	Involved atoms	O–H(H···O)	ρ_c	$\nabla^2\rho_c$	G_C	V_C	H_C
TEW1a	O-H_a	0.9711	0.3590	−2.7944	0.0751	−0.8488	−0.7737
	O-H_b	0.9597	0.3747	−2.8044	0.0826	−0.8663	−0.7837
	O-H_b···π	3.14918	0.0071	0.0220	0.0047	−0.0038	0.0008
TAW1a	O-H_a	0.9748	0.3534	−2.7502	0.0747	−0.8369	−0.7623
	O-H_b	0.9576	0.3773	−2.8180	0.0842	−0.8729	−0.7887
BAW1a	O-H_a	0.97564	0.3523	−2.7403	0.0747	−0.8345	−0.7598
	O-H_b	0.95749	0.3775	−2.8196	0.0842	−0.8733	−0.7891
BAW1a*	O-H_a	0.97515	0.3531	−2.7445	0.0746	−0.8353	−0.7607
	O-H_b	0.95759	0.3772	−2.8253	0.0837	−0.8738	−0.7901
BEW1a	O-H_a	0.97211	0.3578	−2.7792	0.0753	−0.8453	−0.7701
	O-H_b	0.95986	0.3746	−2.8069	0.0824	−0.8666	−0.7842
	O-H_b···π	2.9470	0.0072	0.0226	0.0048	−0.0039	0.0009
TEW1b	O-H_a	0.9596	0.3755	−2.4667	0.0794	−0.8755	−0.7962
	C-H_a···O	2.8657	0.0063	0.0254	0.0053	−0.0042	0.0011
	O-H_b	0.9591	0.3743	−2.8554	0.0791	−0.8721	−0.7929
TAW1b	O-H_b	0.9590	0.3688	−2.8496	0.0763	−0.8649	−0.7887
	O-H_a	0.9633	0.3756	−2.8547	0.0803	−0.8743	−0.7939
	O-H_a ···π	2.7059	0.0119	0.0404	0.0083	−0.0065	0.0018
BAW1b	O-H_a	0.96255	0.3712	−2.8302	0.0782	−0.8640	−0.7858
	O-H_b	0.96110	0.3732	−2.8299	0.0796	−0.8667	−0.7871
	O-H_a ···π	2.6238	0.0099	0.0325	0.0066	−0.0050	0.0016
TEW1c	O-H_a	0.9615	0.3725	−2.8341	0.0791	−0.8667	−0.7876
	O-H_b	0.9603	0.3742	−2.8346	0.0802	−0.8691	−0.7889
	O-H_a ···π	2.5044	0.0087	0.0269	0.0056	−0.0046	0.0011
	O-H_b···π	2.7626	0.0075	0.0229	0.0049	−0.0040	0.0008
TAW1c	O-H_a	0.9586	0.3754	−2.8372	0.0809	−0.8712	−0.7903
	O-H_b	0.9631	0.3715	−2.8337	0.0782	−0.8659	−0.7876
	C-H_a···O	2.7248	0.0050	0.0195	0.0041	−0.0034	0.0007
	O-H_b···π	2.4598	0.0138	0.0474	0.0099	−0.0079	0.0020
BAW1c	O-H_a	0.9605	0.3741	−2.8394	0.0800	−0.8697	−0.7898
	O-H_b	0.9612	0.3730	−2.8327	0.0794	−0.8670	−0.7867
	O-H_a ···π	2.7581	0.0080	0.0248	0.0053	−0.0044	0.0009
	O-H_b···π	2.6579	0.0083	0.0257	0.0054	−0.0045	0.0010

clearly indicating the predominance of V_C over G_C. For further verification of this statement, we plotted the different (G_C and V_C) contributions of H_C separately with ρ_C in Fig. 6. Comparing Figs. 5 and 6, we can clearly identify that both $\nabla^2\rho_C$andG_C show a linear variation with ρ_C. H_C and V_C on the other hand cannot be ascribed to a linear plot. H_C in particular shows a strong deviation in the weak h-bonds. The negative values of H_C signify the accumulation of electron density in the inter-nuclear region displayed also by the increase in the value ofρ_C, which corresponds to the covalent nature [9] of the respective non-covalent O–H···N bonds. For further verification and removing any doubts on the methods of computations, we plot the same graphs with the AIM outputs from MP2 computations. This is also included in Figs. 5 and 6.

Some topological descriptors are shown in Table 5 computed with the help of the DFT method. Corresponding table with computations involving the MP2 method is in Table T4 in the supplementary file. The core valence bifurcation (CVB) indices [38] for N–H···O bonded complexes are positive and for O–H···N bonded complexes are negative indicating stronger interaction in the latter case. The ratio of $-G_C/V_C$ at BCP for O–H···N bonded complexes ranges between 0.5 and 1 indicating partial covalent character [39]. Exception is being the TEW1a complex for computations at the DFT level. On the other hand, this ratio strongly correlates with the ordering of E_{NBO} of those bonds. Similar pattern is observed in H_C /ρ_c ratio and more negative value indicates the stronger h-bonding with more covalent character.

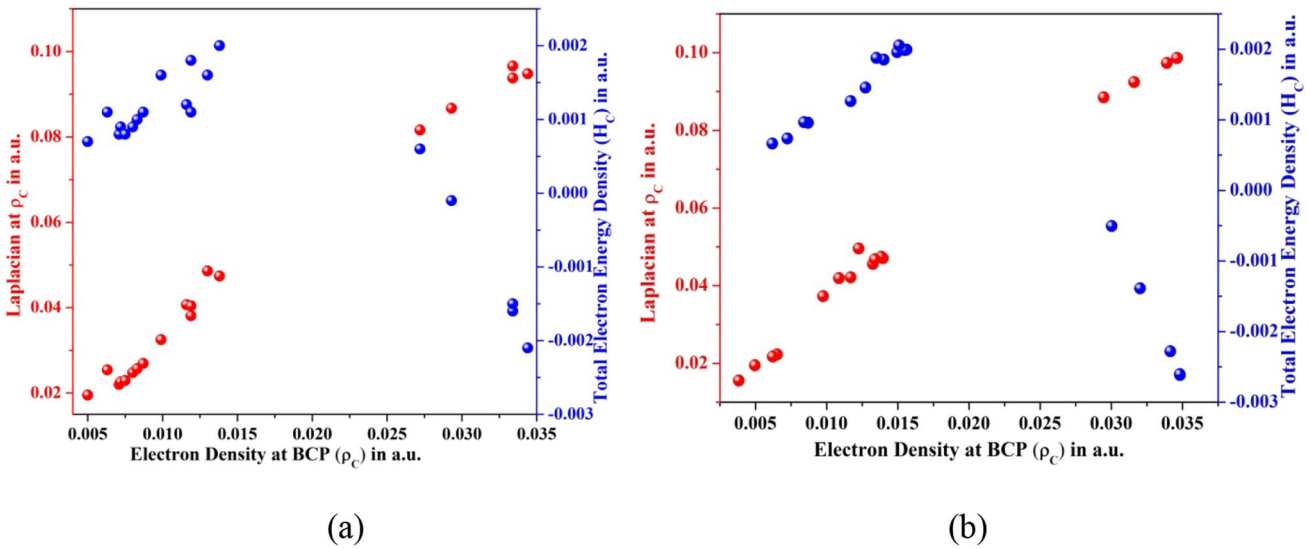

Fig. 5 Variation of Laplacian ($\nabla^2\rho_c$) and Total electron Energy Density (H_C) with electron density (ρ_c) at Bond Critical Point (BCP) for all the hydrogen-bonded monohydrates of THIQ. QTAIM computations are performed at **a**) M06-2X/6–311 + + G (2d, 3p) and **b**) MP2/6–311 + + G (2d, 3p) level of theory. All quantities are in atomic units (a.u.)

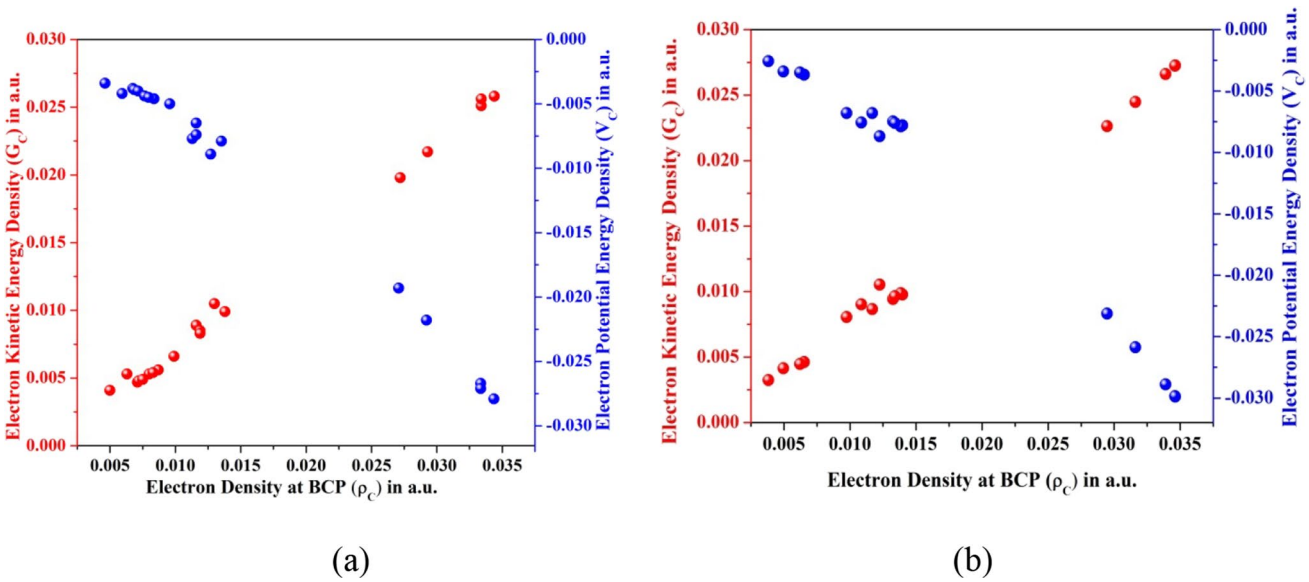

Fig. 6 Variation of Electron Kinetic Energy Density (G_C) and Electron Potential Energy Density (V_C) with electron density (ρ_c) at Bond Critical Point (BCP) for all the hydrogen-bonded monohydrates of THIQ. QTAIM computations are performed at (**a**) M06-2X/6–311 + + G (2d, 3p) and (**b**) MP2/6–311 + + G (2d, 3p) level of theory. All quantities are in atomic units (a.u.)

We want to know how the different interactions change with the variation in BLs. TEW1a and TAW1b are considered where O–H···N, and N–H···O are the primary HBs. In both cases, a weak O–H···π interaction is also present. Then variations of HB bond lengths and associated bond angle as well as $\nabla^2\rho_c$, H_C, G_C, and V_C with ρ_c at BCP of O–H···N and N–H···O h-bonds are presented in Fig. F3 in the supplementary file. Figure F4(a), (b), and (c) correspond to the strong N–H···O and O–H···N interactions while Figure F4(d), (e), and (f) for the weak O–H···π interactions.

Figure F4(a) shows that with the increase in ρ_c the H-bond length decreases rapidly for both types of interactions identically which might hint at identical strength in HBs in TAW1b and TEW1a. But the bond angles show a large variation amongst the two different HBs, where the latter shows more linearity in the participating atoms and amply indicates

Table 5 Some important QTAIM topological descriptors other than H_C to determine the covalency of primary hydrogen bonds of THIQ: H_2O complexes calculated at M06-2X/ 6–311 + + G(2d,3p) level

Complexes	H-Bond	$-G_C/V_C$	H_C/ρ_c	CVB (a.u)
BAW1a	O–H···N	0.92501	−0.06072	−0.04273
TAW1a	O–H···N	0.94001	−0.04807	−0.03787
BAW1a*	O–H···N	0.94541	−0.04414	−0.03402
BEW1a	O–H···N	0.99725	−0.00215	−0.02267
TEW1a	O–H···N	1.02958	0.02099	−0.01489
BAW1b	N–H···O	1.11476	0.07174	0.051759
TAW1b	N–H···O	1.16282	0.10796	0.05212
TEW1b	N–H···O	1.1861	0.12673	0.051247

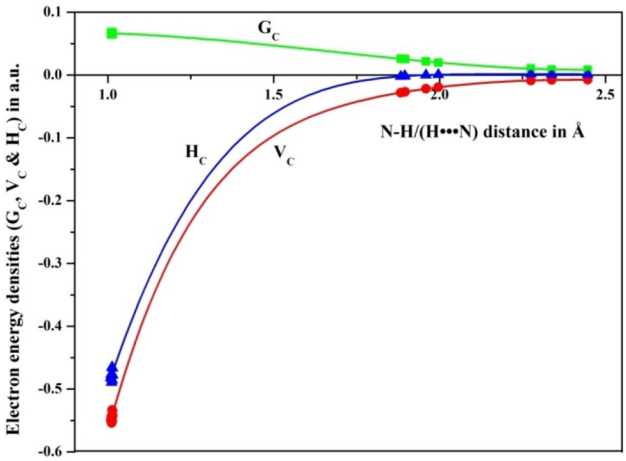

Fig. 7 Variation of three electron energy densities (G_C, V_C, and H_C) at BCP (in a.u) with the change of N–H/(N···H) length (in Å) of different complexes

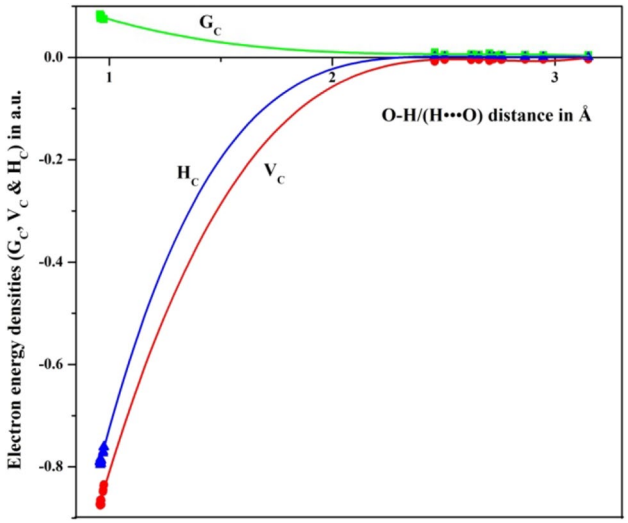

Fig. 8 Variation of three electron energy densities (G_C, V_C, and H_C) at BCP (in a.u) with the change of O–H/(O···H) length (in Å) of different complexes

the latter has a higher binding energy. Here, the variation in bond angles provides a much clearer picture about their differences in bond strength. Figure F4(b) indicates that as the ρ_c increases, the variation of $\nabla^2\rho_c$ and H_C becomes prominent. The rate of change of $\nabla^2\rho_c$ with ρ_c for N–H···O interaction is faster than that of O–H···N interaction. The corresponding variation of H_C with ρ_c of N–H···O interaction is slower than that of O–H···N interaction although H_C became negative for approximately same value of ρ_c. At a lower value of ρ_c, similar variation is observed for G_C and V_C given in Figure F4(c). But as ρ_c increases the variation of G_C become much more than V_C and the variation is faster for N–H···O interaction for both cases.

The change h-bond length with the change of ρ_c is greatly affected by the π-bonding angle in the O–H···π interaction. The change of $\nabla^2\rho_c$, G_C and V_C with ρ_c are almost linear in these types of HBs. But due to the formation of an additional C2-H···O in the TAW1b complex, the O–H···π bond angle changes and we find the change till $\rho_c = 0.0136$ a.u. But the variation of H_C is quite different for π-bond and it seems to affect significantly with bond angle.

We also plot the variation of these energy densities (G_C, V_C, and H_C) with all the NH and OH bond lengths including covalent and non-covalent interactions in Figs. 7 and 8, respectively. Here, covalent interactions are clearly identified over the non-covalent interactions through the values of the respective energies. A close look at the figures indicates that NH covalent bonds are weaker than the OH covalent bonds. On the contrary, if we consider non-covalent interactions N···H bonds show larger strength than the O···H bonds. This can also be concluded from the respective bond lengths as shown in Table 3. We leave out the H···π bonds from this discussion as it is much weaker than the above ones.

In AIM theory, the strength of hydrogen bonding is further verified through the properties of hydrogen atoms in the complexes. In this way, the different types of hydrogen bonding were also identified [40] apart from the conventional ones. The topological criteria for the existence of hydrogen bonding were put forward by Popelier [24] which are already stated earlier. The criteria (i) to (iii) are already verified in the earlier discussions.

We computed the charges on hydrogen atoms in isolated THIQ and water molecules and in the monohydrated complexes by integrating the electron density in the appropriate hydrogen atom regions partitioned by the AIM theory. All these results are listed in Table T5 in the supplementary material. It shows clearly that the hydrogen nuclei are deshielded on hydrogen bond formation. The amount of change ranges between 0.030 and 0.052 a.u. in all the monohydrates for O–H···N and N–H···O type of HBs. This is consistent with earlier studies on different hydrated complexes [40, 41]. The

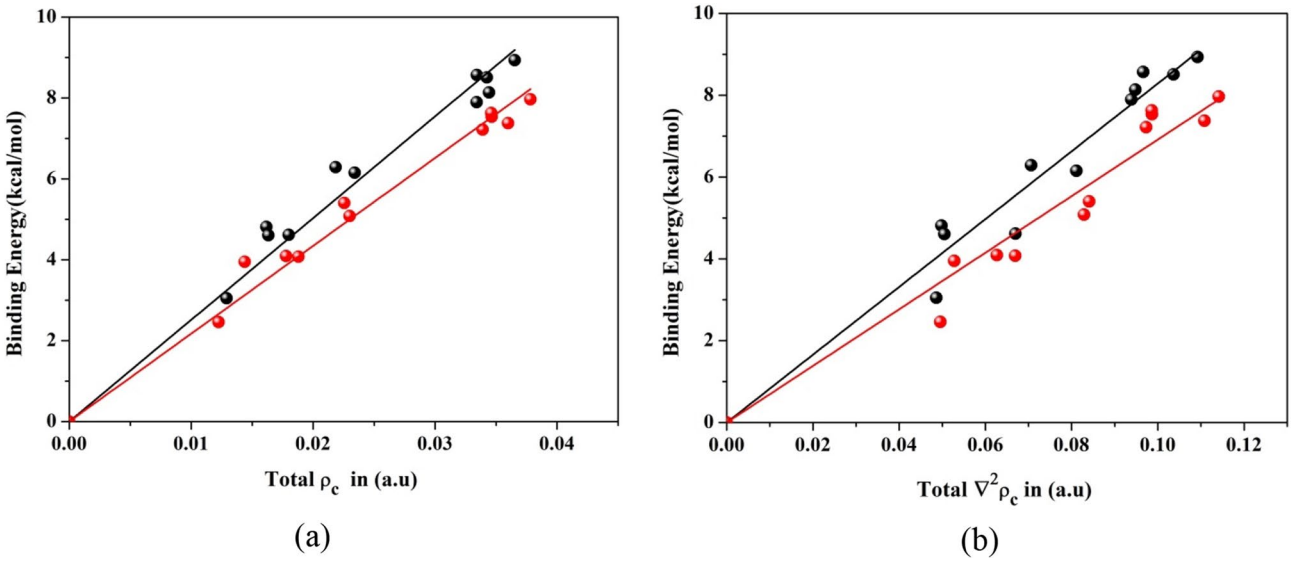

Fig. 9 Relationship between binding energy and **a** total electron density (ρ_c), **b** total Laplacian of electron density ($\nabla^2\rho_c$), at hydrogen bonds critical points for all THIQ:H_2O complexes. All computations are performed with M06-2X/6–311 + + G(2d,3p) (black circle ●) and MP2/6–311 + + G(2d,3p) (red circle ●) basis sets

weak HBs involving pi electron clouds and C-H···O HBs show some discrepancies. The range of change in the magnitude of charge, first moment, volume, and energy depends on the involvement of the hydrogen atom with the h-bond acceptor. Similar variations were also observed in previous studies on hydrogen-bonded complexes [40, 41]. This table also includes the destabilization energy of the H atom. This value ranges between 0.001 and 0.162 a.u. indicating the changes in energy of H atoms participating in the complex formation. Here, also the stronger HBs show consistent data, but the weaker ones again show some unusual variations. The dipolar polarization is measured by the first moment of H atoms taking part in h-bonding. This table shows a decrease in this value, verifying the validity of the seventh criterion put forward by Popelier. In the same table, we also insert the changes observed in the computed values of hydrogen atom volume during the formation of complex from the values in bare THIQ and in the monohydrates. Interestingly, this also satisfies the criteria (vii), validating our earlier observations. In all the cases some complexes belonging to the weaker HBs show some discrepancies.

The strength of hydrogen bonds is also related through electron density and its Laplacian [41–43]. In Fig. 9, the sum of all the electron densities $\Sigma\rho_C$ and $\Sigma\nabla^2\rho_C$ are plotted with the corresponding BEs. The plots show a linear relationship. The correlation coefficient is also shown in the respective plots. The linear regressional analysis yields the following relation. Binding energy = 251.57 $\sum \rho_c$ and Binding energy = 82.87 $\sum \nabla^2\rho_c$ for DFT computations and the respective values for MP2 methods yield 217.29 $\sum \rho_c$ and 69.18 $\sum \nabla^2\rho_c$

Conclusions

The intermolecular non-covalent interactions in all the eleven monohydrates of THIQ are critically analyzed in this article. We successfully identified a variety of hydrogen bonds in the different complexes. The energy densities in the different complexes were partitioned by QTAIM approaches. Some of the hydrogen bonds show partial covalent character through the negative values of H_C as well as the ratio of $-G_C/V_C$. All these are O–H···N type. The value of H_C in the O–H···N bond of TAW1a has a value very close to zero. Corresponding value of $\rho_c = 0.0285$ and bond length of around 1.96 Å may be considered as a turnover point to the partial covalent nature of H-bonds and vice versa. Poppeliar criteria are found to be satisfied in all the complexes. Although some of the weak HBs show some inconsistencies, rehybridization is found to be the dominant interaction in the "b" type complexes rather than hyperconjugation to determine the change of different properties of O-H_a and O-H_b bonds, E_{NBO} and binding energies [26] are compared in all the complexes and their dependence with conformations of bare molecules are discussed. When an OH bond of water remained free in a complex then its bond length decreases from its value in bare water. This is observed in all cases when the OH bond acts as an HB donor only.

Supplementary Information The online version contains supplementary material available at https://doi.org/10.1007/s00894-022-05438-8.

Acknowledgements AC gratefully acknowledges the support received from University Grants Commission through a research Project (F. No. 37-560/2009(SR)) for conducting this work. The authors also

acknowledge the instrumental support from DST (Govt. of India) under the departmental FIST programme of the University of Burdwan (Grant no: SR/FST/PS-II-/2018/52(C)) and University Grants Commission (UGC) for departmental CAS (Grant no. F.530/20/CAS-II/2018(SAP-I)) scheme.

Author contribution Santu Das: literature survey, editing, software handling, data handling, presentation of figures. Abhijit Chakraborty: conceptualisation and visualisation of the problem, writing, reviewing and editing the manuscript, literature survey.

Declarations

Competing interests The authors declare no competing interests.

References

1. Lewis GN (1916) The atom and the molecule. J Am Chem Soc 38:762–785
2. Kollman PA (1977) Noncovalent interactions. Chem Rev 10:365–371. https://doi.org/10.1021/ar50118a003
3. Lopinski GP, Wayner DDM, Wolkow RA (2000) Self-directed growth of molecular nanostructures on silicon. Nature 406:48–51. https://doi.org/10.1038/35017519
4. Autumn K, Sitti M, Liang YA, Peattie AM, Hansen WR, Sponberg S, Kenny TW, Fearing R, Israelachvili JN, Full RJ (2002) Evidence for van der Waals adhesion in Gecko State. Proc Natl Acad Sci USA 99:12252
5. Li D, Zhu Z, Sun DW (2020) Visualization of the in situ distribution of contents and hydrogen bonding states of cellular level water in apple tissues by confocal Raman microscopy. Analyst 145:897–907. https://doi.org/10.1039/C9AN01743G
6. Etim EE, Gorai P, Das A, Chakrabarti SK, Arunan E (2008) Interstellar hydrogen bonding. Adv Space Res 612870–2880. https://doi.org/10.1016/j.asr.2018.03.003
7. Pauling L, Corey RB, Branson HR (1952) The structure of proteins: two hydrogen-bonded helical configurations of the polypeptide chain. Proc Natl Acad Sci USA 37:205
8. Watson JD, Crick FHC (1953) A structure for deoxyribose nucleic acid. Nature 171:737
9. Grabowski SJ (2011) What is the covalency of hydrogen bonding? Chem Rev 111:2597–2625. https://doi.org/10.1021/cr800346f
10. Mahadevi AS, Sastry GN (2016) Cooperativity in noncovalent interactions. Chem Rev 116:2775–2825. https://doi.org/10.1021/cr500344e
11. Zwier TS (1996) The spectroscopy of solvation in hydrogen-bonded aromatic clusters. Annu Rev Phys Chem 47:205–241. https://doi.org/10.1146/annurev.physchem.47.1.205
12. Arunan E, Desiraju GR, Klein RA, Sadlej J, Scheiner S, Alkorta I, Clary DC, Crabtree RH, Dannenberg JJ, Hobza P (2011) Definition of the hydrogen bond (IUPAC recommendations 2011. Pure Appl Chem 83:1637–1641
13. Ghosh S, Wategaonkar S (2020) C-H···Y (Y=N, O, π) Hydrogen bond: a unique unconventional hydrogen bond. J Ind Inst Sc 100:101–125. https://doi.org/10.1007/s41745-019-00145-5
14. Banerjee P, Chakraborty T (2018) Weak hydrogen bonds: insights from vibrational spectroscopic studies. Int Rev Phys Chem 37(1):83–123. https://doi.org/10.1080/0144235X.2018.1419731
15. Weinhold F, Landis CR, Glendening ED (2016) What is NBO analysis and how is it useful? Int Rev Phys Chem 35(3):399–440. https://doi.org/10.1080/0144235X.2016.1192262
16. Alabugin IV, Manoharan M, Peabody S, Weinhold F (2003) Electronic basis of improper hydrogen bonding: a subtle balance of hyperconjugation and rehybridization. J Am Chem Soc 125(19):5973–5987. https://doi.org/10.1021/ja034656e
17. Joseph J, Jemmis ED (2007) Red-, blue-, or no-shift in hydrogen bonds: a unifiedexplanation. J Am Chem Soc 129(15):4620–4632. https://doi.org/10.1021/ja067545z
18. Grabowski SJ (2013) Non-covalent interactions - QTAIM and NBO analysis. J Mol Model 19(11):4713–4721. https://doi.org/10.1007/s00894-012-1463-7
19. Bader RFW (1991) A quantum theory of molecular structure and its applications. Chem Rev 91:893. https://doi.org/10.1021/cr00005a013
20. Bader RFW (1990) Atoms in molecules, a quantum theory. Oxford University Press, Oxford
21. (2007) Quantum theory of atoms in molecules: recent progress in theory and application; Matta, C., Boyd, R. J., Eds.; Wiley-VCH: New York.
22. Grabowski SJ, Sokalski WA, Leszczynski J (2006) The possible covalent nature of N-H….O hydrogen bonds in formamide dimer and related systems: an ab initio study. J Phys Chem A 110:4772–4779. https://doi.org/10.1021/jp055613i
23. Kuznetsov ML (2019) Relationships between interaction energy and electron density properties for homo halogen bonds of the [(A)nY–XX–Z(B)m] type (X = Cl, Br, I), Molecules 24:2733 https://doi.org/10.3390/molecules24152733
24. Koch U, Popelier PL (1995) Characterization of C-H-O hydrogen bonds on the basis of the charge density. J Phys Chem 99:9747. https://doi.org/10.1021/j100024a016
25. Das S, Das L, Chakraborty A (2020) Conformers of 1,2,3,4 –tetrahydroisoquinoline in S0 and S1: an analysis through potential energy surface, hardness principles and vibrational spectroscopy. J Mol Struc 1207:127836. https://doi.org/10.1016/j.molstruc.2020.127836
26. Das S, Chakraborty A (2021) Conformer selective monohydrated clusters of 1,2,3,4 –tetrahydroisoquinoline in S_0: I-Potential energy surface studies, vibrational signatures and NBO analysis. J Mol Struct 1225:129177. https://doi.org/10.1016/j.molstruc.2020.129177
27. Das S, Chakraborty A (2023) Computational investigation of the conformer selective complexes of 1,2,3,4-tetrahydroisoquinoline: ammonia (THIQ: NH_3) in S_0. J Mol Struct 134475. https://doi.org/10.1016/j.molstruc.2022.134475
28. Guchhait N, Banerjee S, Chakraborty A, Nath DN, Patwari GN, Chowdhury M (2004) Structure of hydrated clusters of tetrahydroisoquinoline THIQ–(H_2O) n = 1,3 investigated by jet spectroscopy. J Chem Phys 120:9514–9523. https://doi.org/10.1063/1.1711810
29. Chakraborty A, Guchhait N, Banerjee S, Nath DN, Patwari GN, Chowdhury M (2001) Spectroscopic investigation of tetrahydroisoquinoline in supersonic jet. J Chem Phys 115:5184–5191. https://doi.org/10.1063/1.1394742
30. Parr RG, Yang W (1989) Density-functional theory of atoms and molecules. Oxford University Press, New York
31. Frisch MJ, Head-Gordon M, Pople JA (1990) A direct MP2 gradient method. Chem Phys Lett 166:275–280
32. Walker M, Harvey AJA, Sen A, Dessent CEH (2013) Performance of M06, M06–2X and M06-HF density functionals for conformationally flexible anionic clusters M06 functionals perform better than B3LYP for a model system with dispersion and ionic hydrogen-bonding interactions. J Phys Chem A 117:12590–12600
33. McLean AD, Chandler GS (1980) Contracted Gaussian basis sets for molecular calculations. I. Second row atoms, Z=11–18. J Chem Phys 72:5639–5648. https://doi.org/10.1063/1.438980

34. Gaussian09 (Revision B.1), Frisch MJ, Trucks GW, Schlegel HB, Scuseria GE, Robb MA, Cheeseman JR, Scalmani G, Barone V, Mennucci B, Petersson GA, Nakat-suji H, Caricato M, Li X, Hratchian HP, Izmaylov AF, Bloino J, Zheng G, Sonnenberg JL, Hada M, Ehara M, Toyota K, Fukuda R, Hasegawa J, Ishida M, Nakajima T, Honda Y, Kitao O, Nakai H, Vreven T Jr, Montgomery JA, Peralta J E, Ogliaro F, Bearpark M, Heyd JJ, Brothers E, Kudin KN, Staroverov VN, Kobayashi R, Normand J, Raghavachari K, Rendell A, Burant JC, Iyengar SS, Tomasi J, Cossi M, Rega N, Millam JM, Klene M, Knox JE, Cross JB, Bakken V, Adamo C, Jaramillo J, Gomperts R, Stratmann RE, Yazyev O, Austin AJ, Cammi R, Pomelli C, Ochterski JW, Martin RL, Morokuma K, Zakrzewski VG, Voth GA, Salvador P, Dannenberg JJ, Dapprich S, Daniels AD, Farkas, Foresman JB, Ortiz JV, Cioslowski J, Fox DJ (2009) Gaussian, Inc., Wallingford CT
35. Lu T, Chen F (2012) Multiwfn: a multifunctional wavefunction analyzer. J Comput Chem 33:580–592
36. Bent HA (1961) An appraisal of valence-bond structures and hybridization in compounds of the first-row elements. Chem Rev 61:275–311
37. Johnson ER, Keinan S, Sa'nchez PM, Contreras-Garcı'a J, Cohen AJ, Yang W (2010) Revealing noncovalent interactions. J Am Chem Soc 132:6498–6506. https://doi.org/10.1021/ja100936w
38. Fuster F, Silvi B (2000) Does the topological approach characterize the hydrogen bond? Theor Chem Acc 104:13–21
39. Emamian S, Lu T, Kruse H, Emamian H (2019) Exploring nature and predicting strength of hydrogen bonds: a correlation analysis between atoms-in-molecules descriptors, binding energies, and energy components of symmetry-adapted perturbation theory. J Comput Chem 9999:1–14. https://doi.org/10.1002/jcc.26068
40. Cubero E, Orozco M, Hobza P, Luque FJ (1999) Hydrogen bond versus anti-hydrogen bond: a comparative analysis based on the electron density topology. J Phys Chem A 103:6394. https://doi.org/10.1021/jp990258f
41. Parthasarathi R, Subramanian V, Sathyamurthy N (2005) Hydrogen bonding in phenol, water, and phenol-water clusters. J Phys Chem A 109:843–850. https://doi.org/10.1021/jp046499r
42. Kuznetsov ML (2019) Relationships between interaction energy and electron density properties for homo halogen bonds of the [(A)nY–XX–Z(B)m] type (X = Cl, Br, I), Molecules 24:2733. https://doi.org/10.3390/molecules24152733
43. Kumar PSV, Raghavendra V, Subramanian V (2016) Bader's theory of atoms in molecules (AIM) and its applications to chemical bonding. J Chem Sci 128(10):1527–1536. https://doi.org/10.1007/s12039-016-1172-3